A STUDY OF SODALITE BY PARAMAGNETIC RESONANCE

A Study of Sodalite by Paramagnetic Resonance

By

Robert Lang B. Sc.

A Thesis

Submitted to the Faculty of Graduate Studies

in Partial Fulfilment of the Requirements

for the Degree

Master of Science

McMaster University

April, 1967

Master of Science (1967)

(Physics)

Title: **A Study of Sodalite by Paramagnetic Resonance**

Author: Robert Lang B. Sc. (McMaster University)

Supervisors: Professors C. Calvo, W. R. Datars

Number of Pages: (v) 48

Content:

Single crystals of sodalite have been studied by means of electron paramagnetic resonance (E. P. R.) both at 0.8 cm. and 3 cm. wavelength.

The existence of at least four different E. P. R. spectra was established of which one was attributed to the manganese impurity and a possible model for two other spectra is proposed. It was found that two of the observed spectra disappear upon heat treatment although the bleaching of the characteristic blue colour of sodalite crystals does not appear to be related to any of the spectra studied.

Acknowledgements

The author wishes to thank Professors C. Calvo and W. R. Datars for their guidance and help throughout the course of this research.

Thanks are also extended to Mr. John Vanderkooy and Mr. John S. Moss for providing their know-how and experienced assistance on numerous occasions.

Financial aid was received from the Ontario Research Foundation and the National Research Council of Canada, to whom the author is greatly indebted.

TABLE OF CONTENTS

LIST OF ILLUSTRATIONS

LIST OF TABLES

CHAPTER I

Introduction

Single crystals of sodalite found in nature are typically opaque and blue in colour. When heated to approximately 200°C the blue colour changes to light grey. Upon x-ray bombardment in air the blue colour is reinstated. This property was the original motivation for studying sodalite by paramagnetic resonance since its origin was not understood.

Crystals of the mineral sodalite which were studied in this work were found in an area near Bancroft, Ontario. Its structure was determined by L. Pauling (1930) and T. F. W. Barth (1932) to be cubic with a = 8.9 Å, space group $P\bar{4}3m$, and formula $Na_8Cl_2[AlSiO_4]_6$ per unit cell. The structure consists of a linkage of SiO_4 and AlO_4 tetrahedra of approximately equal numbers to form cage-like cubo-octahedral units. It is not certain, however, as to whether or not there is any ordering in the distribution of Al and Si atoms. This octahedral unit is formed by placing one ring, made up of four tetrahedra, parallel to each of the six { 100 } faces and one ring of six tetrahedra parallel to each of the eight { 111 } faces. These cages are then stacked such that each ring of six tetrahedra is shared by two cages. Thus channels are formed by these six-membered rings which intersect at the corners and centers of

the unit cells to form large cavities. Each cavity is occupied by a chlorine atom which is tetrahedrally co-ordinated by four sodium atoms.

Several experiments on sodalite have been reported recently. Synthetic single crystals of both hydro-sodalite $Na_8(AlSiO_4)_6\ (OH)_2$ and chlorosodalite $Na_8(AlSiO_4)_6\ Cl_2$ were produced by O. K. Mel'nikov, (1965) using hydrothermal synthesis. Electrical and optical properties of single crystal sodalite $Na_8(AlSiO_4)_6\ (OH\ Cl)_2$ have been studied by Yu. V. Shaldin et al, (1966).

CHAPTER II

Theory

1. The Resonance Condition

When a free ion is placed in a magnetic field H_o the Hamiltonian loses its spherical symmetry and the (2J+1) fold degeneracy of an electronic energy level is removed, where J is the total angular momentum quantum number. When H_o is directed along the Z-direction the additional term in the Hamiltonian becomes $H = g\beta H_o J_z$ where g is the Lande g-factor given by

$$g = 1 + \frac{J(J+1) + S(S+1) - L(L+1)}{2J(J+1)} \qquad (2.1)$$

$\beta = \frac{e\hbar}{2mc}$ is the Bohr magneton, m is the mass of the electron and c the velocity of light. L and S are the orbital and spin angular momenta. In the standard J^2, J_z representation H is represented by the matrix $(H_{mn}) = (g\beta H_o m\delta_{mn})$ where m, n = J, J-1..... - (J-1), -J. Consequently, each energy level splits into 2J+1 equally spaced levels with separation $E_m - E_{m-1} = g\beta H_o$. To produce resonance one makes use of the interaction between the magnetic moment $\vec{\mu} = -\frac{g|e|\hbar}{2mc}\vec{J}$ of the atom and the alternating magnetic field $H_x = H_x^o \cos \omega t$ of the electromagnetic radiation applied at right angles to H_o, say along the x-direction. This interaction gives rise to a perturbation:

$$H' = - \mu_x H_x = g\beta H_x^o J_x \cos \omega t = \frac{1}{2} g\beta H_x^o [J_+ + J_-] \cos \omega t$$

which only connects states m and m' where m' = m±1.

To conserve energy of the total system one must have

$$\hbar \omega = g\beta H_o \simeq \frac{2 \times 10^{-20} \times 10^4}{3 \times 10^{10} \times 6 \times 10^{-27}} \text{ [ergs]} \simeq 1 \text{ [cm}^{-1}\text{]}$$

Therefore for H_o = 10 kilogauss the radiation used is typically in the microwave region. To ensure continuous absorption of energy from the microwave radiation one needs a steady rate of transitions from a lower to a higher energy level, say from E_{m-1} to E_m. From time dependent perturbation theory it is known that the transition probability from state a to state b is given by

$$P_{a \to b} = \frac{2\pi}{\hbar} |(b |V| a)|^2 \delta(E_a - E_b - \omega) = P_{b \to a}$$

where V is the applied perturbation. Therefore no net amount of energy is absorbed unless the population of the lower energy level remains always higher than the population of the upper energy level. Otherwise any initial population difference would exponentially decay under the influence of the microwave radiation and no continuous signal could be observed. Therefore the spin system must be connected to an effective "heat reservoir" with which it is in thermal equilibrium at all times such that the populations are described by

$$\frac{N_a}{N_b} = \exp \frac{-(E_a - E_b)}{kT} \qquad (2.2)$$

where k is the Boltzmann constant.

For systems in the solid state this heat reservoir is provided by the lattice and T is called the spin temperature.

2. Paramagnetic Ions in Solids

Since the energy level structure of free atoms and ions is well understood from atomic spectroscopy it seems reasonable to attempt to arrive at the structure of atoms in solids by treating the effect of the crystalline environment as a perturbation on the free atom. To do so one must know the strength of the crystalline interactions relative to the various interactions of the electrons in the free atom. The Hamiltonian of a free atom with N electrons takes the form:

$$H = \sum_{\kappa=1}^{N} \left(\frac{P_\kappa^2}{2m} - \frac{Ze^2}{r_\kappa}\right) + \frac{1}{2} \sum_{\kappa,j}{}' \frac{e^2}{r_{\kappa j}} + V_{LS} + V_{SS} + V_N + V_Q \qquad (2.3)$$

where the various terms are listed roughly in order of decreasing magnitude. The first two summations consist of the kinetic energy and the Coulomb interaction of the electrons with the nucleus and among themselves.

V_{LS} is the magnetic interaction of the spin of the electrons with their orbital angular momentum, which for Russel-Saunders coupling can be written as $V_{LS} = \lambda L \cdot S$ where L and S are total angular momentum and spin of all electrons in the atom.

$$V_{SS} = \sum_{j<\kappa} \frac{\vec{s}_j \cdot \vec{s}_\kappa}{r_{j\kappa}^3} - \frac{3\vec{r}_{j\kappa} \cdot \vec{s}_j}{r_{j\kappa}^5} \qquad (2.4)$$

If the nucleus has spin I and quadrupole moment Q there are two additional

interactions of the electrons with the nucleus:

$$V_N = 2\gamma\beta\beta_N \sum_\kappa \left[\frac{(\vec{l}_\kappa - \vec{s}_\kappa).\vec{I}}{r_\kappa^3} + \frac{3(\vec{r}_\kappa.\vec{s}_\kappa)(\vec{r}_\kappa.\vec{I})}{r^5} + \frac{8\pi}{3}\delta(r_\kappa)\vec{s}_\kappa.\vec{I} \right] \tag{2.5}$$

and

$$V_Q = \frac{e^2Q}{2I(I-1)} \sum_\kappa \left[\frac{I(I+1)}{r_\kappa^3} - \frac{3(\vec{r}_\kappa.\vec{I})^2}{r_\kappa^5} \right] \tag{2.6}$$

Where β_N and γ are the nuclear magneton and the nuclear gyromagnetic ratio.

The strength of the electrostatic interaction between the paramagnetic electrons of an atom in a solid and its diamagnetic neighbours ranges from ~ 0.01 cm^{-1} to 50,000 cm^{-1}. Because of this large range different methods have to be used to handle different cases:

1. The crystalline interaction large compared to Russel-Saunders coupling: The individual electron interacts more strongly with the crystal than with the other electrons of the atom. One first determines the Stark splitting of the single electron energy levels due to the crystalline field and then, using the wave functions associated with each Stark level, one determines further term splittings due to inter-electronic interactions. This situation applies to complexes of the 4d and 5d groups.

2. The crystalline interaction small compared to Russel-Saunders coupling but large compared to spin orbit coupling: One starts by calculating the splitting of energy levels characterized by the total orbital angular

momentum L by the crystalline field. This usually leads to partial or total quenching of the orbital angular momentum. One then proceeds to obtain further splitting of levels with different total angular momentum J due to spin orbit coupling. This situation applies to iron group complexes.

3. Crystalline interaction small compared to spin orbit coupling: The total angular momentum quantum number J of the free atom state remains a good quantum number in the solid state. One couples states of constant J to the crystalline field to obtain the level splitting. This approximation applies to rare earth complexes.

Once it is decided at which point in the approximation the crystalline interaction enters into the Hamiltonian of the free atom a method first presented by Bethe (1929) enables one to determine the number and the degeneracies into which an energy level of the free atom splits due to a crystalline field of given symmetry. The method also yields the angular dependence of the proper zero order wave functions which in turn gives the z-component of the angular momentum of the particular state. The method is based on the following principle: When a free atom is placed in a solid the spherical symmetry of its Hamiltonian is reduced to the symmetry of the point group at the site of the atom in the solid. The wave functions belonging to each energy level of the free atom form a basis for an irreducible representation of the group of the Schroedinger equation of the free atom, which is the full rotation group. Thus each energy level in the free atom has associated with it an irreducible representation of the full rotation group, which is also a representation of the crystal point group since it is a subgroup of the

full rotation group. This representation is now in general reducible with respect to the crystal point group into its irreducible components. The number of irreducible components gives the number of energy levels and the dimension of each irreducible representation gives the degeneracy of each energy level into which the free atom energy level splits. The basis functions of each irreducible representation which are linear combinations of the original basis functions i.e. of spherical harmonics times radial functions, represent the proper zero order wave functions, which have to be used in any further perturbation calculation. Since only symmetry enters the above arguments the results obtained are independent of the nature or strength of the crystalline interaction. However, it gives no information about the size of the splittings. A typical example is a 3d electron in a cubic octahedral site where the crystal field is stronger than the spin orbit coupling. 3d electrons are described by the spherical harmonics Y_2^m which are also basis functions for the 5-dimensional irreducible representation $D^{(2)}$ of the full rotation group. $D^{(2)}$ can be reduced with respect to the octahedral group as follows:

$$D^{(2)} = \Gamma_3 + \Gamma_5 \qquad (2.7)$$

where Γ_3 and Γ_5 are 2 and 3 dimensional irreducible representations of the octahedral group. If the basis functions of $D^{(2)}$ are denoted by $\psi_2^2, \psi_2^1, \psi_2^0, \psi_2^{-1}, \psi_2^{-2}$ then the basis functions of Γ_3 are ψ_2^0, $\frac{1}{\sqrt{2}}(\psi_2^2 + \psi_2^{-2})$ and those of Γ_5 are ψ_2^1, ψ_2^{-1}, $\frac{1}{\sqrt{2}}(\psi_2^2 - \psi_2^{-2})$. From electrostatic repulsion considerations it can easily be seen from the contours of the wave functions that Γ_5 corresponds to the lower and Γ_3

to the upper energy level. The splitting is typically of the order 10^4 cm^{-1} as found experimentally by optical absorption. The expectation value of the orbital angular momentum component L_z is zero for $\frac{1}{\sqrt{2}}(\psi_2^2 \pm \psi_2^{-2})$. Since only the ground state Γ_5 is occupied at normal temperatures a 3d electron acts as if it had $l = 1$ rather than $l = 2$ as can be seen by taking expectation values of L_z. Thus there is partial quenching of orbital angular momentum. It can be fully quenched by reducing the symmetry of the lattice site to tetragonal. In this case the Γ_3 and Γ_5 levels are split further by reducing the Γ_3 and Γ_5 representations with respect to the tetragonal group, which is a subgroup of the octahedral group:

$$\begin{aligned} \Gamma_3 &= G_1 + G_3 \\ \Gamma_5 &= G_4 + G_5 \end{aligned} \tag{2.8}$$

where G_1, G_3, G_4 are one-dimensional and G_5 is the two-dimensional irreducible representation of the tetragonal group.

The basic functions are:

for G_1: ψ_2^0

G_3: $\frac{1}{\sqrt{2}}(\psi_2^2 + \psi_2^{-2})$

G_4: $\frac{1}{\sqrt{2}}(\psi_2^2 - \psi_2^{-2})$

G_5: $\frac{1}{\sqrt{2}}(\psi_2^1 + \psi_2^{-1}), \frac{1}{\sqrt{2}}(\psi_2^1 - \psi_2^{-1})$

Clearly $\langle L_z \rangle = 0$ for each of these wave functions.

Taking into account the spin of the electron the total number of states which the electron can occupy is given by:

$$\Psi_{\alpha 2^{\pm}} = \frac{\alpha}{\sqrt{2}} \left(\psi_2^{\,2} \pm \psi_2^{\,-2} \right)$$

$$\Psi_{\beta 2^{\pm}} = \frac{\beta}{\sqrt{2}} \left(\psi_2^{\,2} \pm \psi_2^{\,-2} \right)$$

$$\Psi_{\alpha 1^{\pm}} = \frac{\alpha}{\sqrt{2}} \left(\psi_2^{\,1} \pm \psi_2^{\,-1} \right)$$

$$\Psi_{\beta 1^{\pm}} = \frac{\beta}{\sqrt{2}} \left(\psi_2^{\,1} \pm \psi_2^{\,-1} \right)$$

$$\Psi_{\alpha o} = \alpha \psi_2^{\,o}, \qquad \Psi_{\beta o} = \beta \psi_2^{\,o}$$

Where α and β are spin functions corresponding to $S_z = 1/2$ and $S_z = -1/2$ respectively.

When the above wave functions are used as zero order wave functions to calculate the effect of spin orbit coupling to first order using the formula

$$\Psi_m' = \Psi_m - \sum_{\kappa}' \Psi_\kappa \frac{(\Psi_\kappa \,|\lambda L \cdot S|\, \Psi_m)}{E_\kappa - E_m} \tag{2.10}$$

the new wave functions of the ground state are:

$$\Psi'_{\alpha 2-} = \alpha \left[\frac{1}{\sqrt{2}} \left(\psi_2^{\,2} - \psi_2^{\,-2} \right) - \frac{\lambda}{\sqrt{2}\,\Delta} \left(\psi_2^{\,2} + \psi_2^{\,-2} \right) \right] + \frac{\lambda}{\sqrt{2}\,\delta} \beta \, \psi_2^{\,-1}$$

$$\Psi'_{\beta 2-} = \beta \left[\frac{1}{\sqrt{2}} \left(\psi_2^{\,2} - \psi_2^{\,-2} \right) + \frac{\lambda}{\sqrt{2}\,\Delta} \left(\psi_2^{\,2} + \psi_2^{\,-2} \right) \right] \tag{2.11}$$

$$- \frac{\lambda}{\sqrt{2}\,\delta} \alpha \, \psi_2^{\,1}$$

where Δ and δ are the splittings as indicated in Fig. 2.1

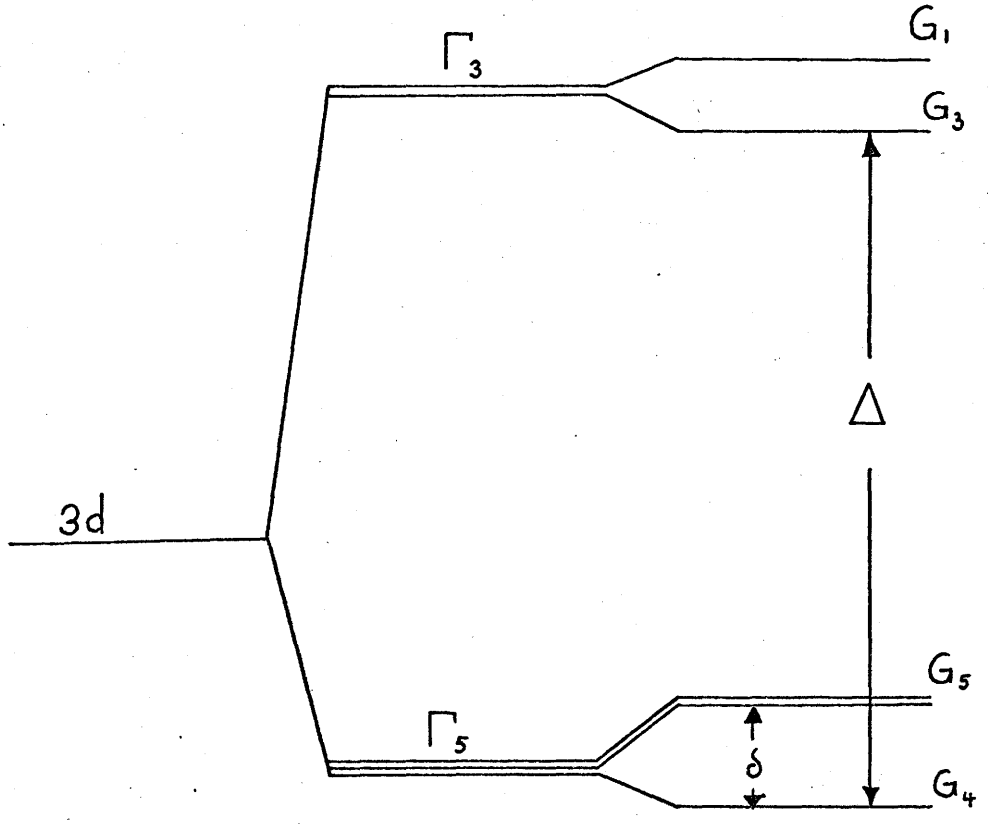

Fig. 2.1: Splitting of a 3d energy level by a large cubic and a small tetragonal field

The expectation values of the orbital angular momentum $\langle L_z \rangle$ now become

$$(\psi'_{\alpha 2-} \mid L_z \mid \psi'_{\alpha 2-}) = -4\frac{\lambda}{\Delta} - \frac{1}{2}\left(\frac{\lambda}{\delta}\right)^2$$

$$(\psi'_{\beta 2-} \mid L_z \mid \psi'_{\beta 2-}) = 4\frac{\lambda}{\Delta} + \frac{1}{2}\left(\frac{\lambda}{\delta}\right)^2 \qquad (2.12)$$

Thus the angular momentum which was quenched out by the tetragonal crystal field is reinstated to a small extent by the spin orbit coupling.

When a magnetic field H is applied along the z-direction the

energy difference between the two ground state Zeeman levels becomes to first order in $\frac{\lambda}{\Delta}$ and $\frac{\lambda}{\delta}$:

$$(\Psi'_{\alpha 2-} | (L_z + \varepsilon_e S_z)\beta H_z | \Psi'_{\alpha 2-})$$

$$- (\Psi'_{\beta 2-} | (L_z + g_e S_z)\beta H_z | \Psi'_{\beta 2-}) \qquad (2.13)$$

$$= [g_e - 8(\frac{\lambda}{\Delta})]\beta H_z = g \beta H_z$$

Where g_e is the free electron g-factor and β is the Bohr magneton. Therefore both the crystalline field and spin orbit coupling have profound effects on the spectroscopic splitting factor g which for the free ion is given by (2.1).

3. The Effective Spin Hamiltonian

The effective spin Hamiltonian describes the experimental resonance data obtained from the lowest group of energy levels of a paramagnetic center without requiring detailed knowledge of the strength and symmetry of the crystalline field or spin orbit coupling. An effective spin quantum number S is postulated such that 2S + 1 gives the number of levels between which microwave transitions are induced under an applied magnetic field. It was shown in the previous section that these electronic ground states are complicated mixtures of spin and orbital wave functions and hence the spectroscopic splitting factor g does not correspond to a "spin only" value but depends on the strength of the spin orbit coupling and the symmetry and direction of the crystal field with respect to the magnetic field. Since the g-factor relates

the magnetic moment $\vec{\mu}$ to the effective spin vector $\vec{S}$ it can be represented by a second rank symmetric tensor $\overline{\overline{g}}$ such that

$$\vec{\mu} = \beta \, \overline{\overline{g}} . \vec{S}$$

and the Zeeman interaction $-\vec{\mu}.\vec{H}$ can be written in the principal axis system of ghe g-tensor as

$$H = \beta[g_{xx} S_x H_x + g_{yy} S_y H_y + g_{zz} S_z H_z]$$

When the perturbation $H = \lambda L \cdot S + \beta H \cdot L$ is carried to second order, terms arise which are quadratic in the effective spin operator and the coefficients form again a second rank symmetric tensor and the interaction can be written as

$$D[S_z^2 - \frac{1}{3} S(S+1)] + E(S_x^2 - S_y^2)$$

in the principal axis system. Similarly it is seen from the expression for the electron nucleus interaction

$$H_{IS} = \frac{8\pi}{3} \gamma_e \gamma_N \hbar^2 \vec{I}.\vec{S} \, \delta(r) + \frac{\gamma_c \gamma_N \hbar^2}{r_3} [\frac{3(\vec{I}\cdot\vec{r})(\vec{S}\cdot\vec{r})}{r_2} - \vec{I}.\vec{S}]$$

that $(\psi(r)|H_{IS}|\psi(r)) = \sum_{\alpha\alpha}, A_{\alpha\alpha'} S_\alpha I_{\alpha'}$

which can be written as

$$H_{IS} = A_{xx} I_x S_x + A_{yy} I_y S_y + A_{zz} I_z S_z$$

where $|\psi(r)\rangle$ is the spatial part of the electron wave function, and γ_e and γ_N are the electron and nuclear gyromagnetic ratio. If $g\beta H >> A_{ii}$ off-diagonal elements can be neglected since they only add an amount $\frac{|A_{ii}|^2}{g\beta H}$ to the energy and first order perturbation yields an additional

term $A_{zz}\ m_I\ m_S$ to each energy level and hence splits it into 2I + 1 components. Since the selection rule $|\Delta m_S| = 1, |\Delta m_I| = 0$ applies there are 2I + 1 different transition frequencies for every single transition before electron-nucleus interaction was taken into account. The total spin Hamiltonian can now be written as

$$H = \beta[g_{xx}\ S_x\ H_x + g_{yy}\ S_y\ H_y + g_{zz}\ S_z\ H_z] + D[S_z^2 - \tfrac{1}{3}(S)(S+1)]$$

$$+ E(S_x^2 - S_y^2) + A_{xx}\ I_x\ S_x + A_{yy}\ I_y\ S_y + A_{zz}\ I_z\ S_z.$$

From this expression the energy levels can be obtained by writing down the matrix of H in a convenient representation and solving the secular equation.

CHAPTER III

Experimental Procedure and Apparatus

1. The E. P. R. Spectrometer

E. P. R. experiments were carried out at 0.8 cm and 3 cm and at temperatures ranging from 1.3°K to 500°K. Preliminary experiments at 0.8 cm were done using essentially the same spectrometer as described earlier by J. S. Leung (1964), except that the Princeton model JB4 was replaced by a specially designed phase sensitive detector and narrow band amplifier tuned to operate at 97 c.p.s. with a bandwidth of approximately 3 c.p.s. Also the diode bridge rectifier which previously supplied the grid voltage for the reflex klystron was found to be a major source of klystron noise and replaced by a 90 volt battery.

The principle of operation of this spectrometer is illustrated in Fig. 3.1: The microwave power generated by the klystron enters arm 1 of the magic Tee after passing through an isolator, a variable attenuator, and a frequency meter. The power is then divided into arms 2 and 3 of the Tee. Arm 3 is terminated with a matched load and a slide screw tuner which allows one to vary the phase and amplitude of the wave which is reflected back into the Tee. The wave reflected back from the cavity through arm 2 is mixed with the wave reflected from the slide screw tuner and enters both arm 1, where it is lost in the isolator, and arm 4 where it is detected by a crystal diode. The slide screw tuner

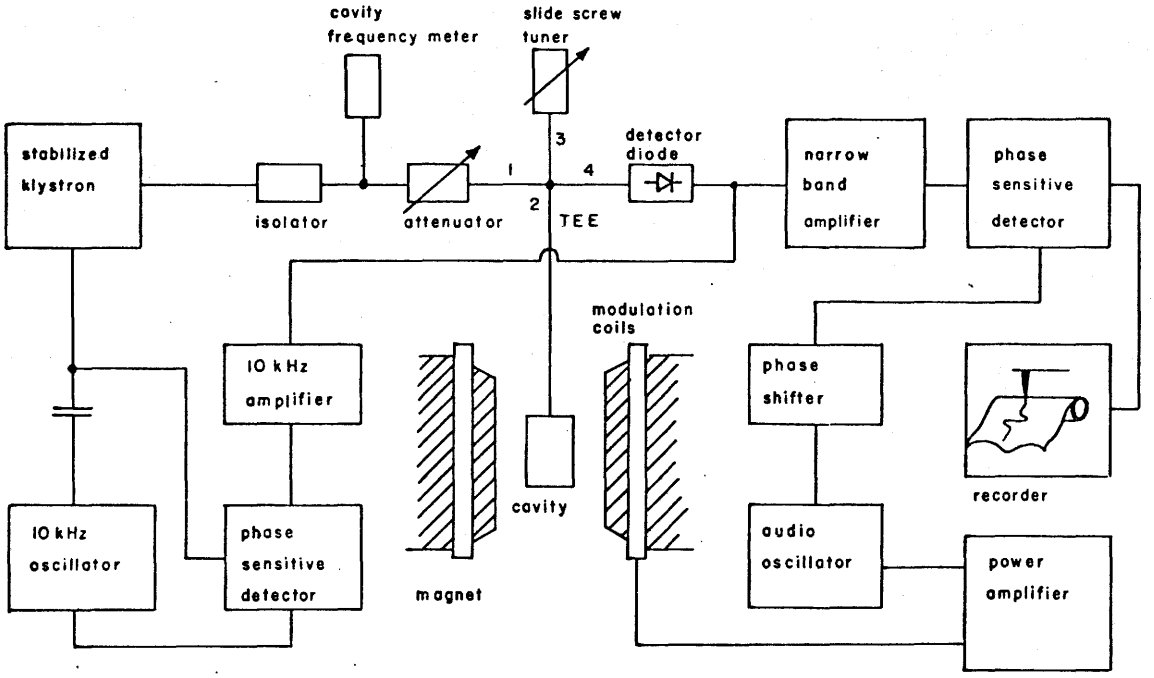

Fig·3·1 BLOCK DIAGRAM OF SPECTROMETER

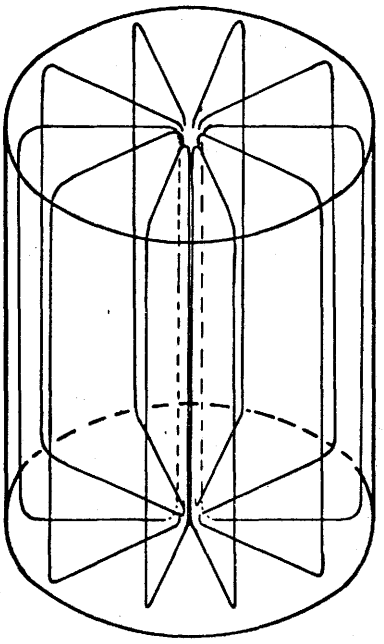

FIG·3·2 H-FIELD CONFIGURATION IN TE011 MODE

was set to detect pure absorption and to give the crystal diode a constant d.c. bias of about 20 millivolts. As the magnetic field passes through the resonance condition the change in the real part of the cavity impedance changes the power level in arm 4 which constitutes the absorption signal.

To discriminate the signal better against random fluctuations in the microwave power level magnetic field modulation was employed which ensured that apart from Fourier components caused by random noise the output at the modulation frequency was zero unless there was resonance. The signal picked up by the crystal detector was fed into a tuned narrow band amplifier and then phase sensitively rectified. The recorded signal was then proportional to the derivative of the paramagnetic resonance absorption line.

An automatic frequency control network operating at 10 kilocycles was used to lock the frequency of the klystron output to the resonant frequency of the sample cavity.

The 0.8 cm data presented in this thesis were obtained with a Varian model V-4503 spectrometer. The 3 cm data were obtained by combining an X-band microwave bridge with the electronic detection system described above for the 0.8 cm spectrometer. Magnetic field measurements were accomplished with a Rawson rotating coil gaussmeter Series 820 which had an accuracy of 0.1% and which was calibrated by nuclear magnetic resonance of protons. In order to eliminate any error in the measured microwave frequency the magnetic field at which the paramagnetic resonance of a trace of DPPH occurred was measured after

every experiment and compared with the calculated magnetic field based on the known g-factor of 2.0036 for DPPH. By multiplying every measured magnetic field value by the ratio

$$\frac{H \text{ (calculated for DPPH)}}{H \text{ (measured for DPPH)}}$$

it was made certain that the ratio $\frac{\omega}{H}$ was correct to 0.1% in all experiments.

2. The Microwave Cavity

To conduct experiments at liquid helium temperatures using 100 KHz magnetic field modulation, a specially designed microwave cavity had to be constructed. The sensitivity considerations which have to be taken into account in the design of a microwave cavity can be summarized as follows:

(a) The output noise of a crystal detector can be written as:

$$P_N = \left(\frac{\alpha I_o^2}{f} + 1 \right) kT\Delta\nu \qquad (3.1)$$

where I_o is the rectified current, f is the modulation frequency around which the bandwidth $\Delta\nu$ is centered i.e. the bandwidth of the narrow band amplifier.

Equation (3.1) makes it desirable to choose f as high as possible. In the present case f = 100 KHz. Since the magnetic field modulation has to penetrate the walls of the cavity a skin depth calculation is necessary to determine the maximum allowable thickness of the cavity walls.

In the approximation for good conductors the classical skin depth is given by

$$\delta \simeq \left[\frac{2\rho}{\mu\omega}\right]^{1/2} \quad \text{(m.k.s.)}$$

where ρ is the resistivity of the cavity walls, $\omega = 2\pi f$ and μ is the permeability $= 1.26 \times 10^{-6}$ $\left[\frac{\text{volt. sec.}}{\text{Amp. m}}\right]$. For silver

$$\delta = \left[\frac{2 \times 1.6 \times 10^{-8}}{1.26 \times 10^{-6} \times 2\pi f}\right]^{1/2} \text{[meters]}$$

and thus becomes

$$= 0.2 \text{ mm. for } f = 100 \text{ KHz}$$

and

$$= 10^{-3} \text{ mm. for } f = 40 \text{ GHz}$$

Therefore the thickness d of the cavity walls has to be in the range 10^{-3} mm. $< d <$ 0.2 mm. These conditions were satisfied with the cavity made of a silver coated glass cylinder which was inserted into a Kel-F holder, as shown in Fig (3.3). The disadvantages of high frequency field modulation are the enormous eddy currents induced in the cavity and dewar walls which lead to high boil off rates of the refrigerants. Also in order to observe undistorted line shapes the relaxation time of the paramagnetic sample must be less than $\frac{1}{f}$. Smaller (1951). The cavity resonates in the TE011 mode. This mode has a high Q and the r.f. field configuration Fig. (3.2) allows easy frequency tuning by means of a non-contact tunable end wall.

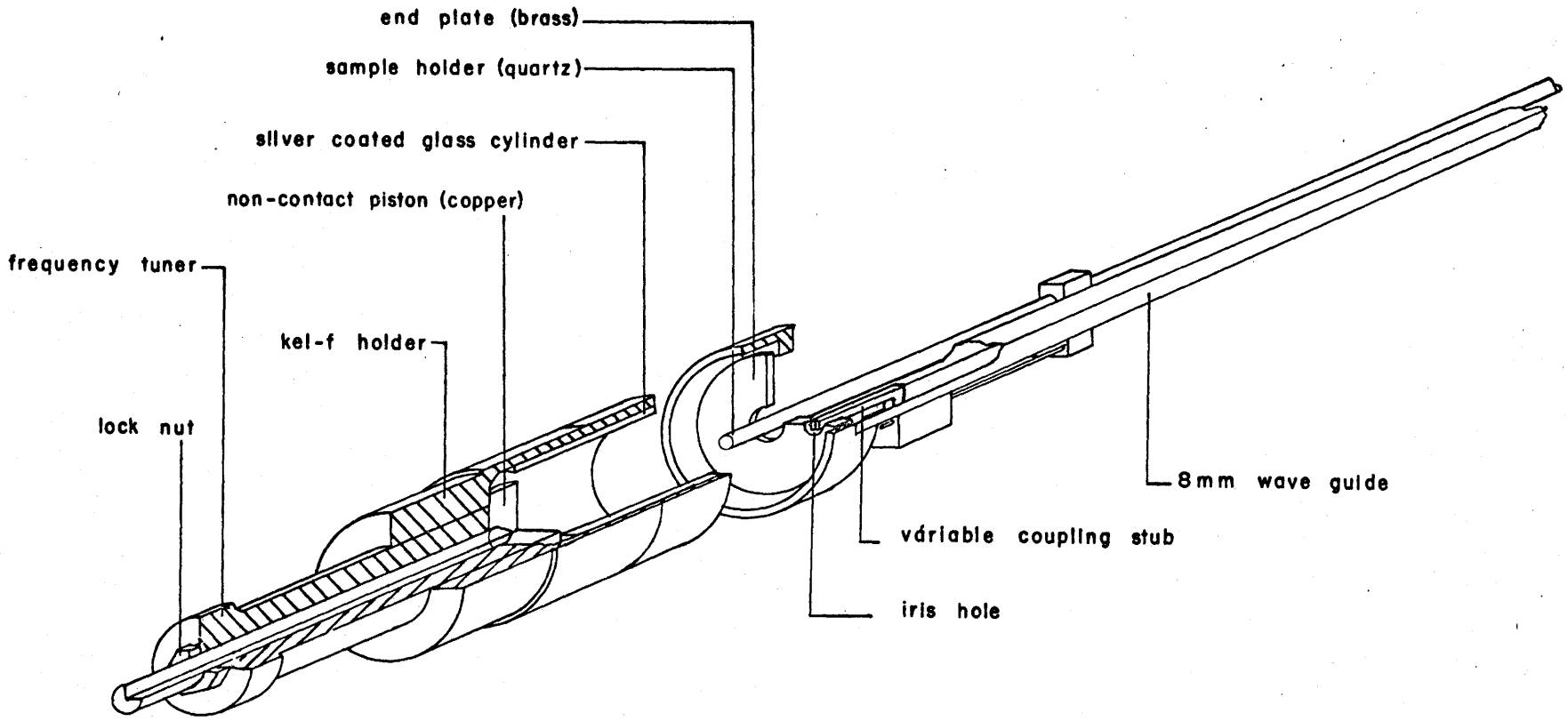

Fig. 3·3 THE TE 011 MICROWAVE CAVITY

(b) In the spectrometers used in this work the crystal detectors operate in the square law region i.e. the rectified current output is proportional to the incident microwave power. However, since the crystal detector is kept at a constant d.c. bias it can be shown that the change in output current ΔI is proportional to the change in the microwave electric field ΔE to first order in ΔE:

$$\Delta I \propto (E_{bias} + \Delta E)^2$$

$$\approx E_{bias}^2 + 2E_{bias}\Delta E$$

Solving for ΔE in terms of the coupling coefficient of the microwave cavity it can be shown (Feher 1957) that maximum sensitivity requires near critical coupling of the cavity. Also in order to observe the dispersion signal it is necessary to operate the cavity near critical coupling. For these reasons it is desirable to have a variable coupling device on the cavity. This was accomplished by a sliding Kel-F stub which had a small piece of copper wire inserted in the end which could be moved in and out of the iris hole of the cavity during an experiment.

3. Sample Mounting and Alignment

All crystals were aligned either on a precession or on a Weissenberg camera. The typical size of a single crystal of sodalite which was used for 8 mm cavities was approximately 1 x 1 x 1 $mm.^3$. The size used for the X-band cavity was approximately 3 x 3 x 2 mm. It was found that crystals having two faces which intersected at a 90°

angle could be aligned very easily since those faces invariably turned out to be {100} faces. Once two such faces were identified the crystal could be oriented by optical methods to within 1/2 of a degree. Once aligned with x-rays on the goniometer head the crystal was glued to the end of a quartz rod of 2 mm. o. d. such that the direction of the quartz rod was parallel to the particular crystalline axis of interest. The quartz rod was inserted along the axis of the cylindrical cavity such that the sample was positioned in the center of the cavity where the microwave magnetic field is maximum. When a particular crystalline plane was scanned the sample was rotated in situ with respect to the fixed direction of the magnetic field.

4. Spectrographic Analysis of Sodalite

A semiquantitative spectrographic analysis of the sodalite crystals used in this study was carried out by A. Mykytiuk of the National Research Council of Canada and found to contain the following approximate impurity concentrations:

Table 3.1

Impurity	Concentration in %
B	0.03 - 0.003
Mg	0.1 - 0.01
Mn	0.3 - 0.03
Ga	0.3 - 0.03
Fe	1.0 - 0.1
Cu	0.003 - 0.0003
Ag	0.001 - 0.0001
Ca	1.0 - 0.1

Among these only Mn, Fe, and Cu would be expected to give rise to E. P. R. signals and then only if they are in the proper oxidation state.

CHAPTER IV

Results and Discussion

1. Spectra

The observed paramagnetic resonance lines can be classified according to intensity, line width, and line separation into five separate spectra which will be denoted by I, II, III, IV, V.

(a) Spectrum I:

By far the most intense signal is obtaind for spectrum I. The angular variation of I was studied by recording spectra every 5° over a range of 180° both in the {100} and {110} planes. Plots of line position versus crystal orientation are shown in Figures 4.1, 4.2 and 4.3 It can be seen that the number of observed lines reduces to two in the ⟨100⟩ and ⟨110⟩ directions. For 0.8 cm microwave radiation the line separation is 20 gauss in the [100] direction and 47 gauss in the [110] direction. For 3 cm radiation the separations are 76 and 170 gauss respectively. The ratios of the respective splittings are $\frac{76}{20} = 3.80$ and $\frac{170}{47} = 3.62$. The inverse ratios of the magnetic fields at which these resonances occur are 3.94 and 3.85 respectively. Thus it appears that the line separations obey approximately a $\frac{1}{H}$ relationship. However, it is also possible that a properly chosen combination of zero field splitting with a Zeeman term would yield the above ratios. Along the ⟨111⟩ directions all lines coalesce. The line width measured between points of highest slope on the absorption

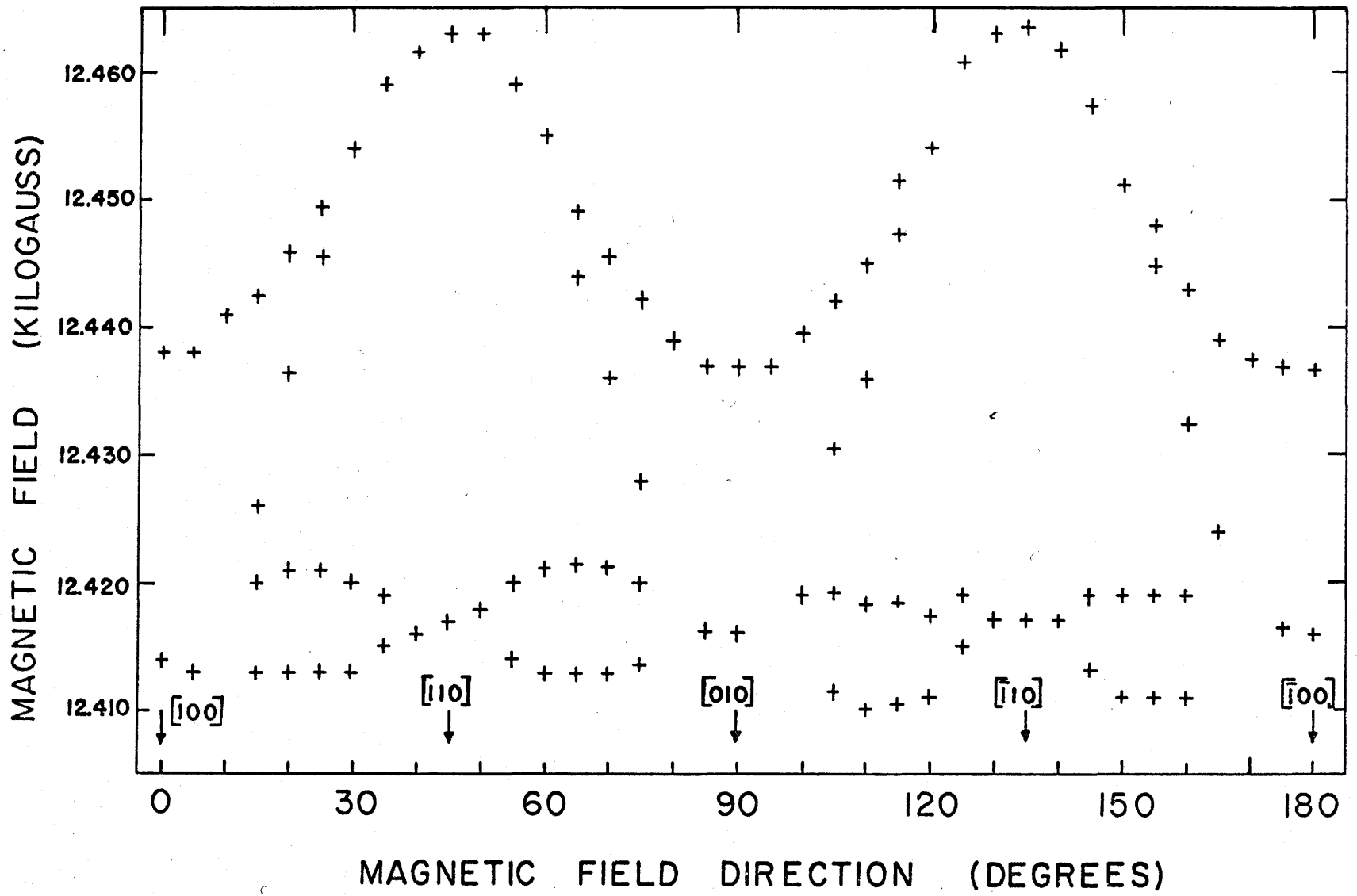

Fig. 4.1 Angular variation of line positions of spectrum I in {100} plane. ν = 34.876 GH$_z$

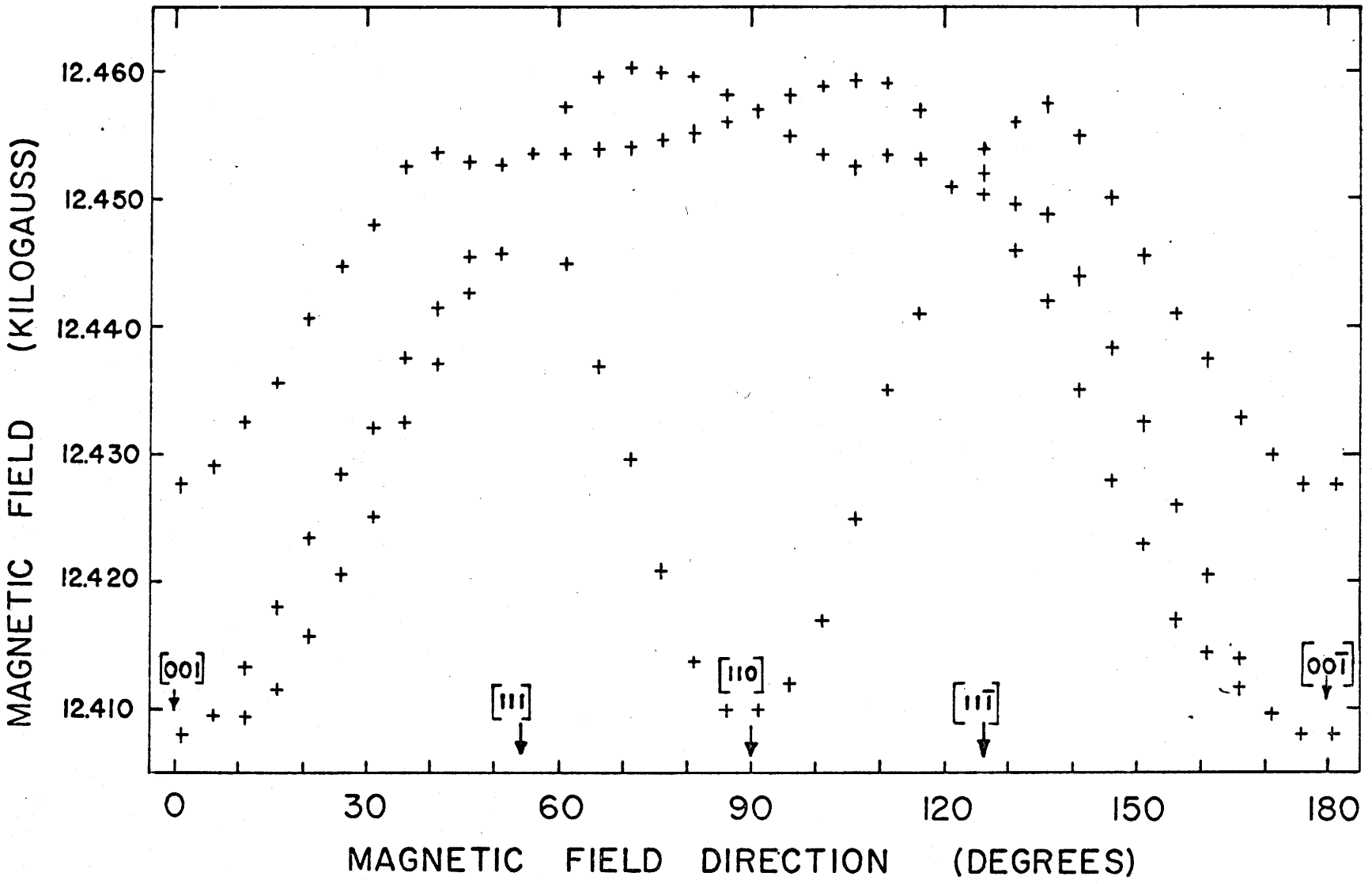

Fig. 4.2 Angular variation of line positions of spectrum I in {100} plane. ν = 34.876 GHz.

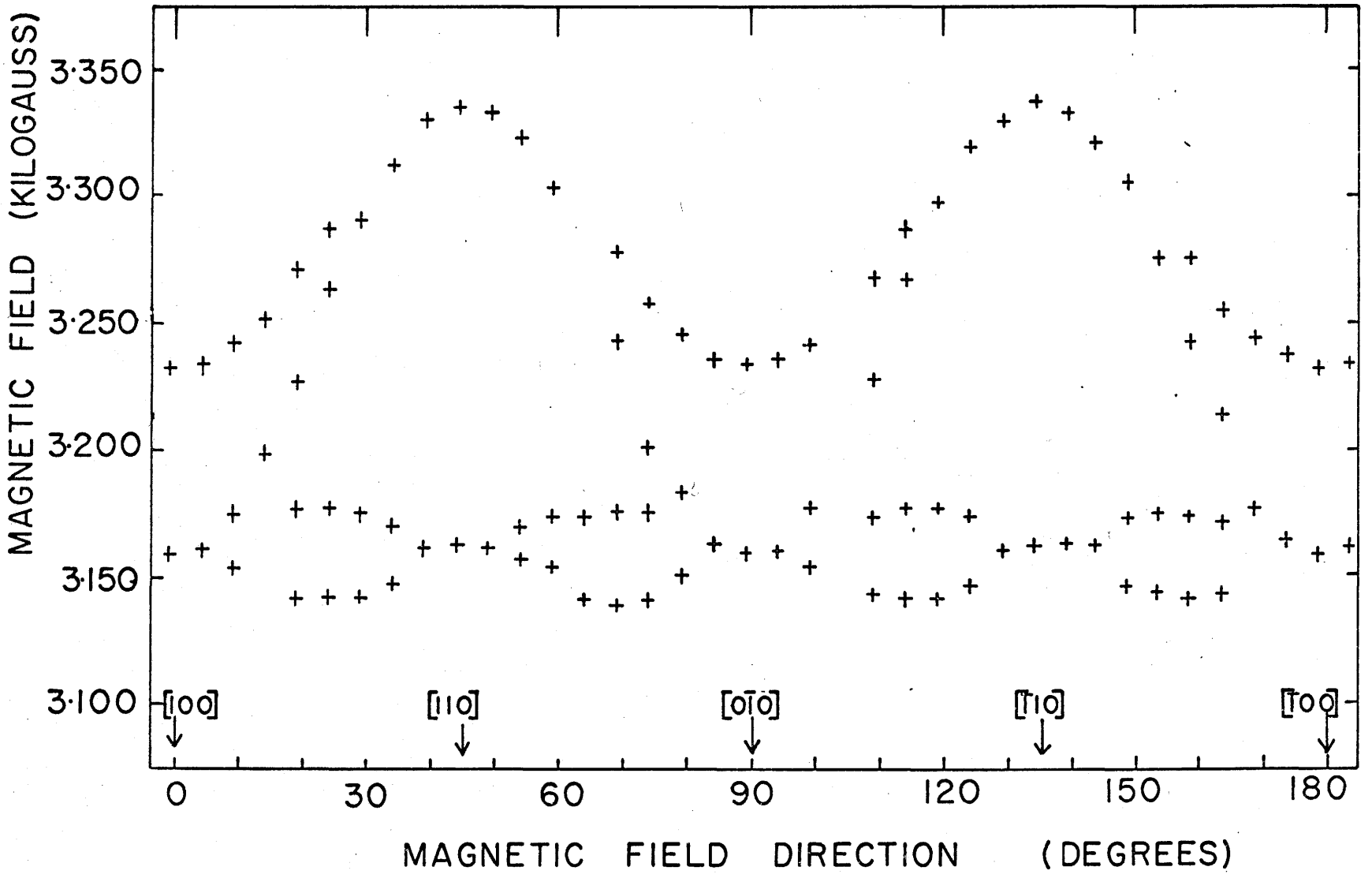

Fig. 4.3 Angular variation of line positions of spectrum I in {100} plane. ν = 9.079 GHz.

curve is approximately 6 gauss at 0.8 cm and 20 gauss at 3 cm wavelength. In the range from -200°C to + 200°C the spectrum was found to be essentially independent of temperature.

The concentration of spins which give rise to spectrum I was determined by comparing the derivative curves of the absorption lines with those of a standard supplied by the Varian Co. The fact that $\int_{-\infty}^{\infty} f(x)\,dx$ is proportional to the number of spins was used, where $f(x)$ is the line shape of the absorption curve. Since $\int_{-\infty}^{\infty} \chi \frac{\partial f(x)}{\partial x}\,dx \propto \int_{\infty}^{\infty} f(x)\,dx$ it was easy to relate the shape of the derivative curve of the absorption line which is recorded in the experiment and the actual absorption line. The difference in the filling factors $\eta = \int_V H_1^2\,dV$ of the standard and the sodalite sample was also taken into consideration and the ratio of the two was found to be approximately 2.5. This method of determining spin concentrations yielded a value of 10^{19} spins per cm^3 which is equivalent to 1 spin per 100 unit cells.

(b) Spectrum II

Spectrum II is about an order of magnitude less intense than I. The {100} and {110} planes were studied by recording spectra at 5° intervals but since the line widths were larger than the line separations for most orientations it was impossible to determine unambiguously the angular variation of the spectrum. Table 4.1 shows the line positions along the ⟨100⟩ and ⟨110⟩ directions.

Table 4.1

frequency of microwave radiation	line positions along 100 (kilogauss)	line positions along 110 (kilogauss)
34.870 ± 0.005 GHz	12.933	12.791
	12.744	12.651
	12.064	12.263
	11.895	12.096
9079 ± 2 MHz	3.771	not observable
	3.547	
	2.883	
	2.725	

The line widths are approximately 60 gauss for both 0.8 cm and 3 cm wavelength.

The following heat treatment caused spectrum II to disappear: A sample was heated at a temperature of 900°C and a pressure of 0.1 microns for 72 hours. Subsequently it was sealed vacuum tight in a quartz tube and quenched in water at room temperature. The resulting spectrum is shown in Fig. 4.4 and was recorded at approximately the same signal level as spectrum II in Fig. 4.5. Spectrum II never re-appeared even after exposing the sample to air and irradiating it with x-rays for several days.

(c) Spectrum III

The angular variation of III was studied in the {100} and {110}

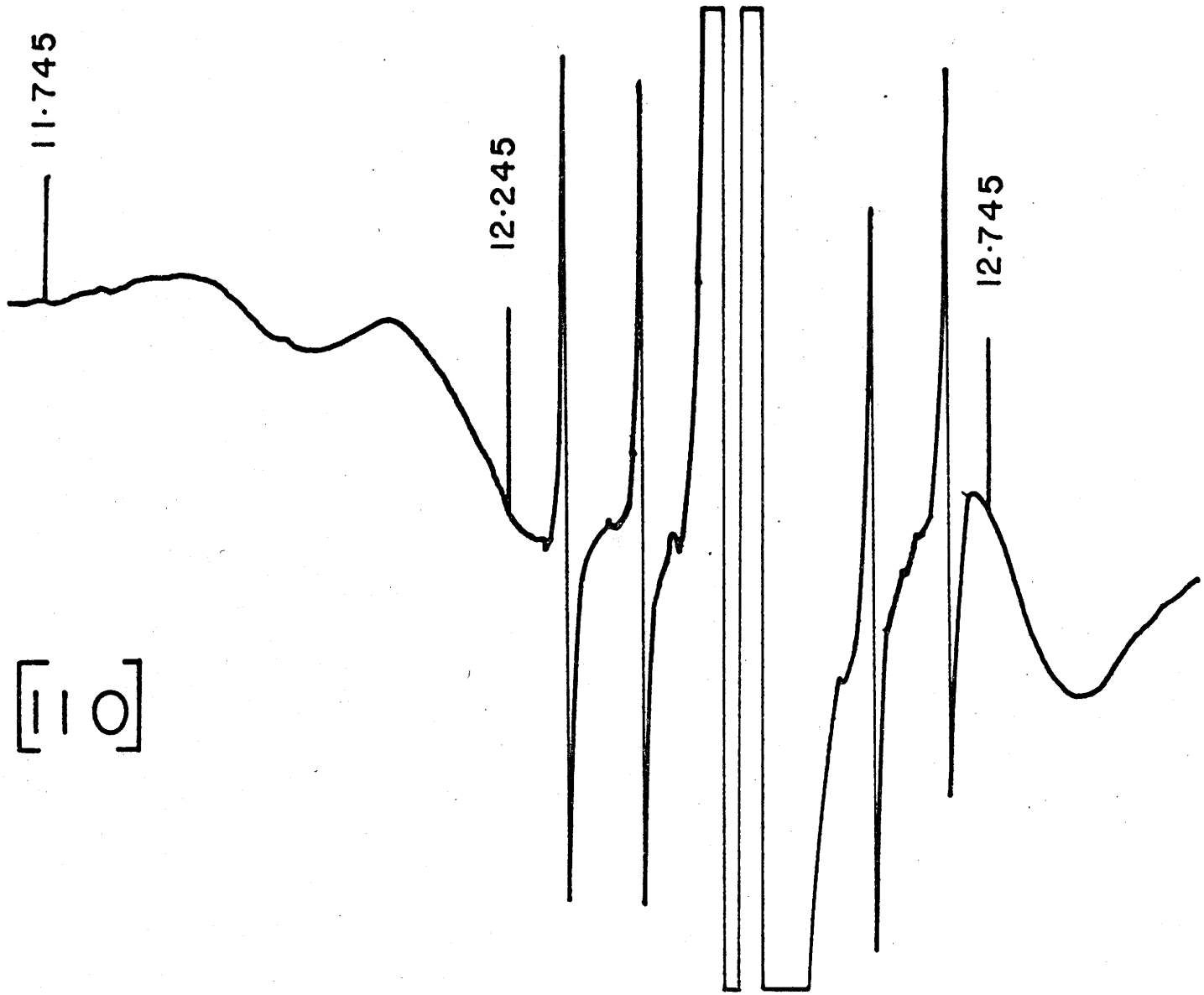

Fig. 4.4 Spectrum IV obtained from heat treated sample
ν = 34.876 GHz.

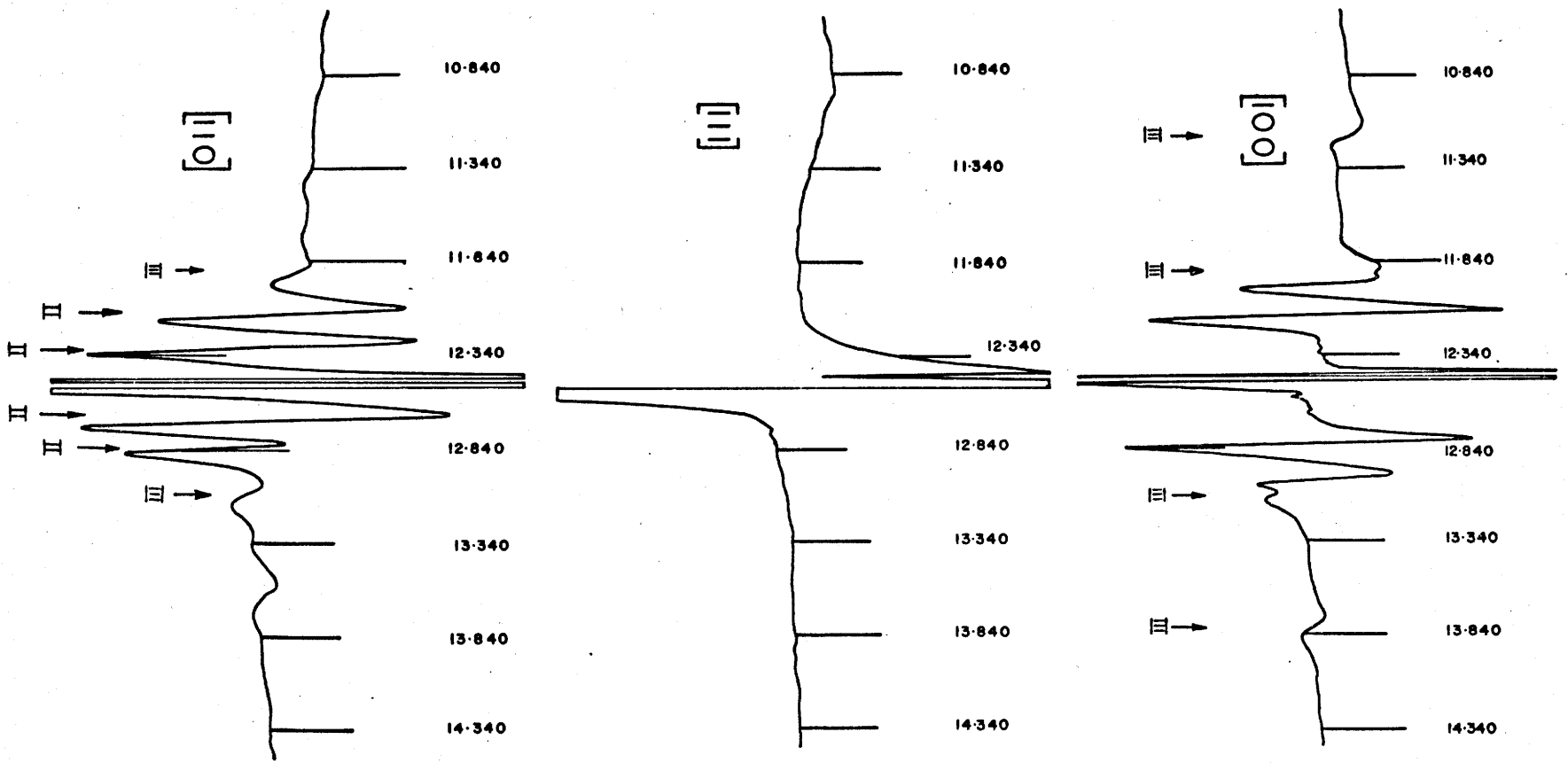

Fig. 4.5 Spectra II and III with the magnetic field along [100], [111], and [110] direction. ν = 34.876 GHz.

planes. The results are plotted in Figures 4.6 and 4.7. No lines could be observed in a region extending from approximately 12 to 13 kilogauss, due to superposition with spectrum II. The line width was measured to be 95 gauss at 0.8 cm. The sensitivity of the 3 cm spectrometer was not sufficient to observe III. Spectrum III also disappeared upon the heat treatment described in (b) and does not reappear after X-irradiation in air.

(d) Spectrum IV

Spectrum IV is isotropic and became only easily observable after the sample was heat treated and II was eliminated.[1] Only four lines are observable in Fig. 4.4. Due to the high intensity of spectrum I any lines falling into the region of I cannot be recorded. The spectrum is attributed to Mn^{2+} which exists in the sample as an impurity of concentration 0.3 - 0.03% and its nuclear spin of $I = \frac{5}{2}$ gives rise to $2I + 1 = 6$ hyperfine lines. It is clear that there must be two more lines between the $m = -\frac{3}{2}$ and the $m = \frac{3}{2}$ transitions since these lines are separated by exactly three line spacings. As was mentioned in section 3 of Chapter II the hyperfine interaction adds a term Am_I to the resonant magnetic field so that the hyperfine coupling constant A can be obtained by measuring the separation between two hyperfine lines. Therefore A = 80 gauss.

---

1 It was found that the signal intensity obtained from IV was up by a factor of 20 after the heat treatment from what it was before.

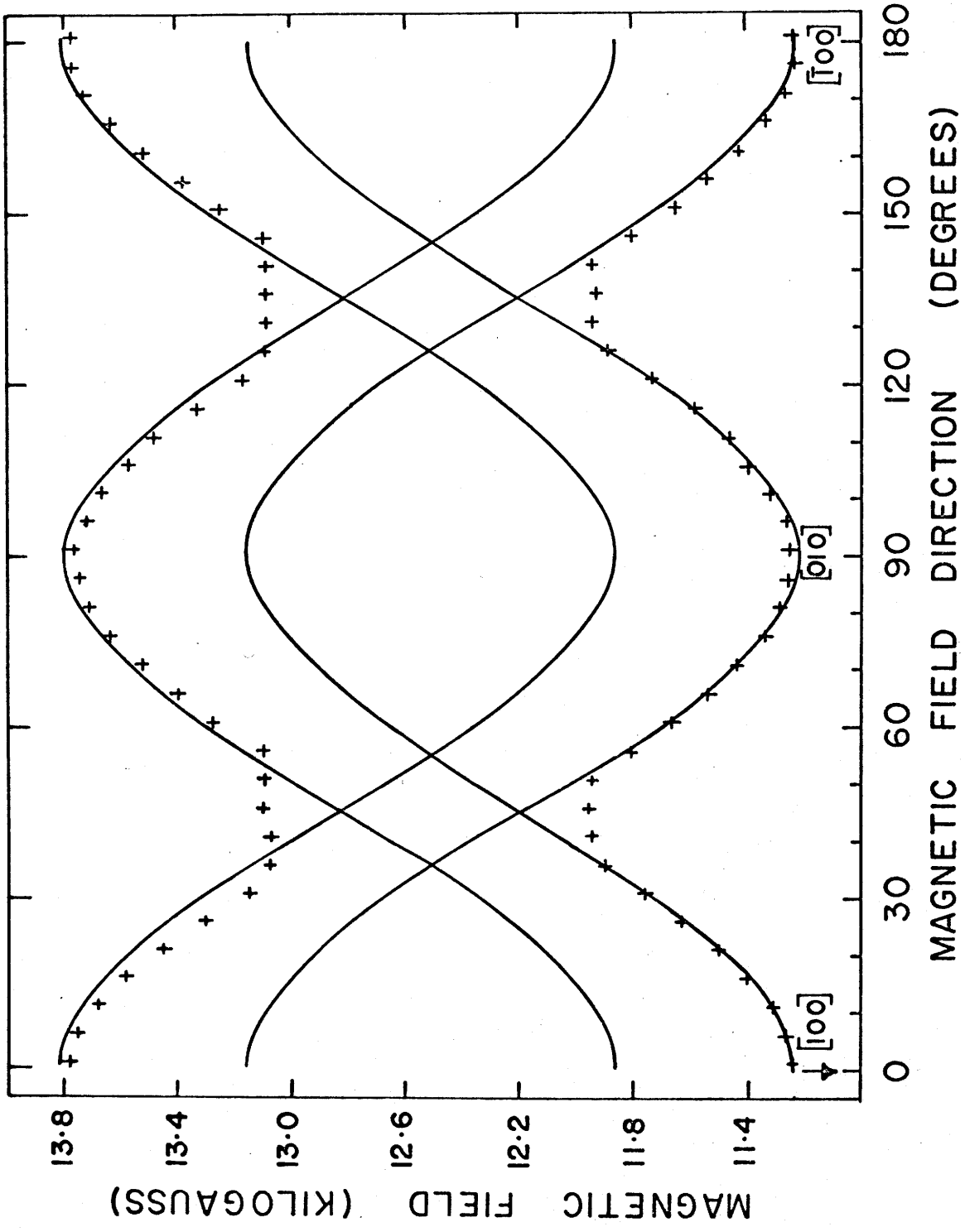

Fig. 4.6 Angular variation of position of the outermost lines of spectrum III in the {100} plane. The solid line represents the theoretical calculation. ν = 34.876 GHz.

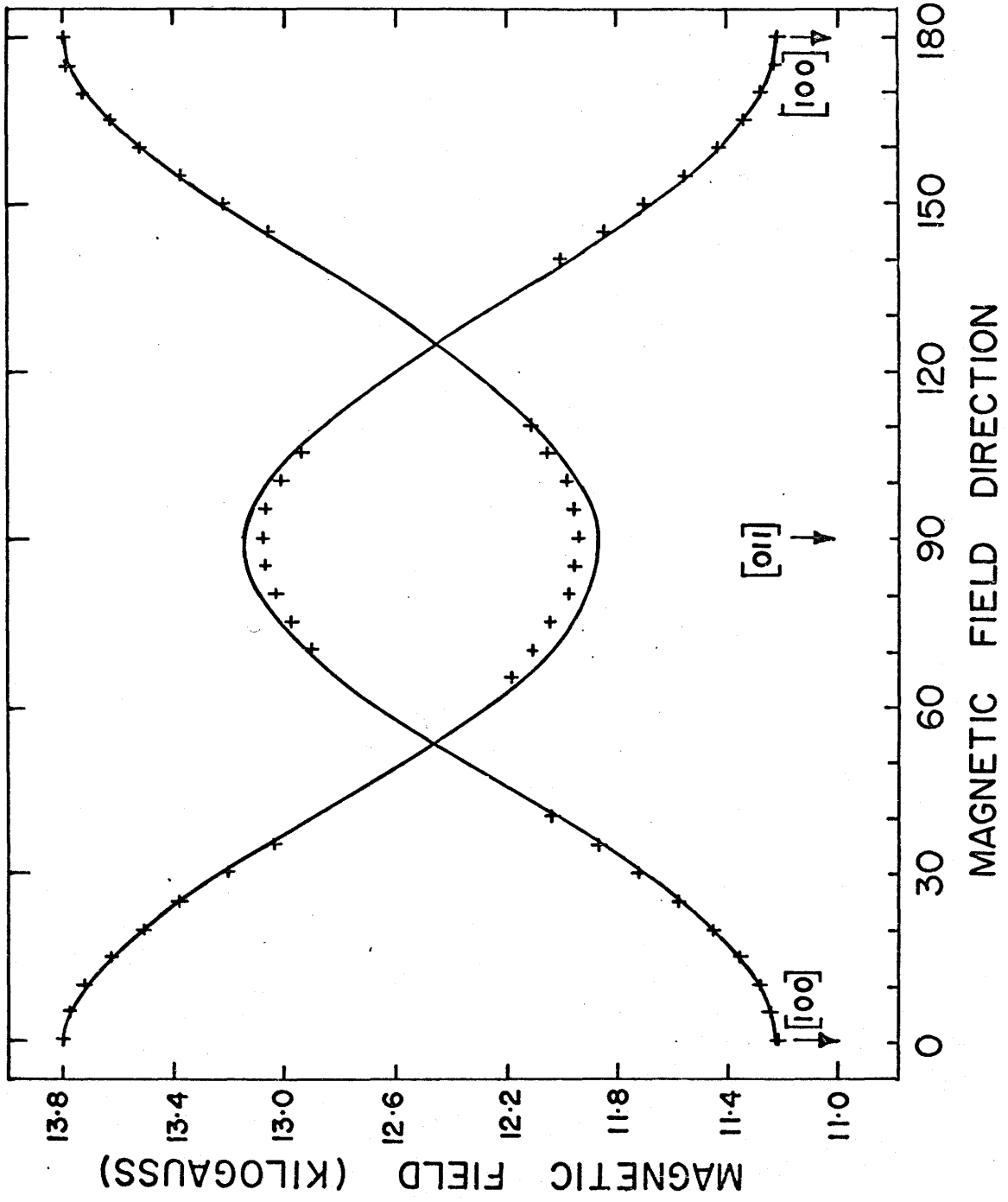

Fig. 4.7 Angular variation of position of the outermost lines of spectrum III in the {110} plane. The solid curve represents the theoretical calculation. ν = 34.876 GHz.

(e) Spectrum V

Spectrum V was obtained at a temperature of 1.3°K and is shown in Fig. 4.8 for a random orientation. The spectrum extends over the same range of magnetic field as III, but is much more intense than III. The lines do not have the familiar derivative shape and the positions vary with orientation of the crystal.

2. Discussion of Results

Attempts to determine the origin of spectrum I were unsuccessful. Of all the impurities in the crystal listed in Table 3.1 only Fe has a concentration which is of the order of the spin concentration measured for spectrum I. The only ionic state of Fe which gives rise to a spectrum at room temperature is Fe^{3+} with a ground state of $^6S_{5/2}$. The sixfold degenerate ground state $^6S_{5/2}$ remains an S-state for crystalline fields which are weaker than Russel-Saunders coupling, as is the case for the iron group transition elements. Therefore this state remains unsplit by the crystalline field to arbitrarily high order. However, Van Vleck and Penney (1934) have shown that simultaneous crystal field and spin orbit interaction produces a splitting of S-states at higher order perturbation. Abragam and Pryce (1951) have suggested the magnetic interaction between the five 3d electrons making up the $^6S_{5/2}$ state as a more likely mechanism to split the S-state energy level. Hence fine structure consisting of five lines ought to exist and experimentally determined spin Hamiltonian parameters for the fine structure are

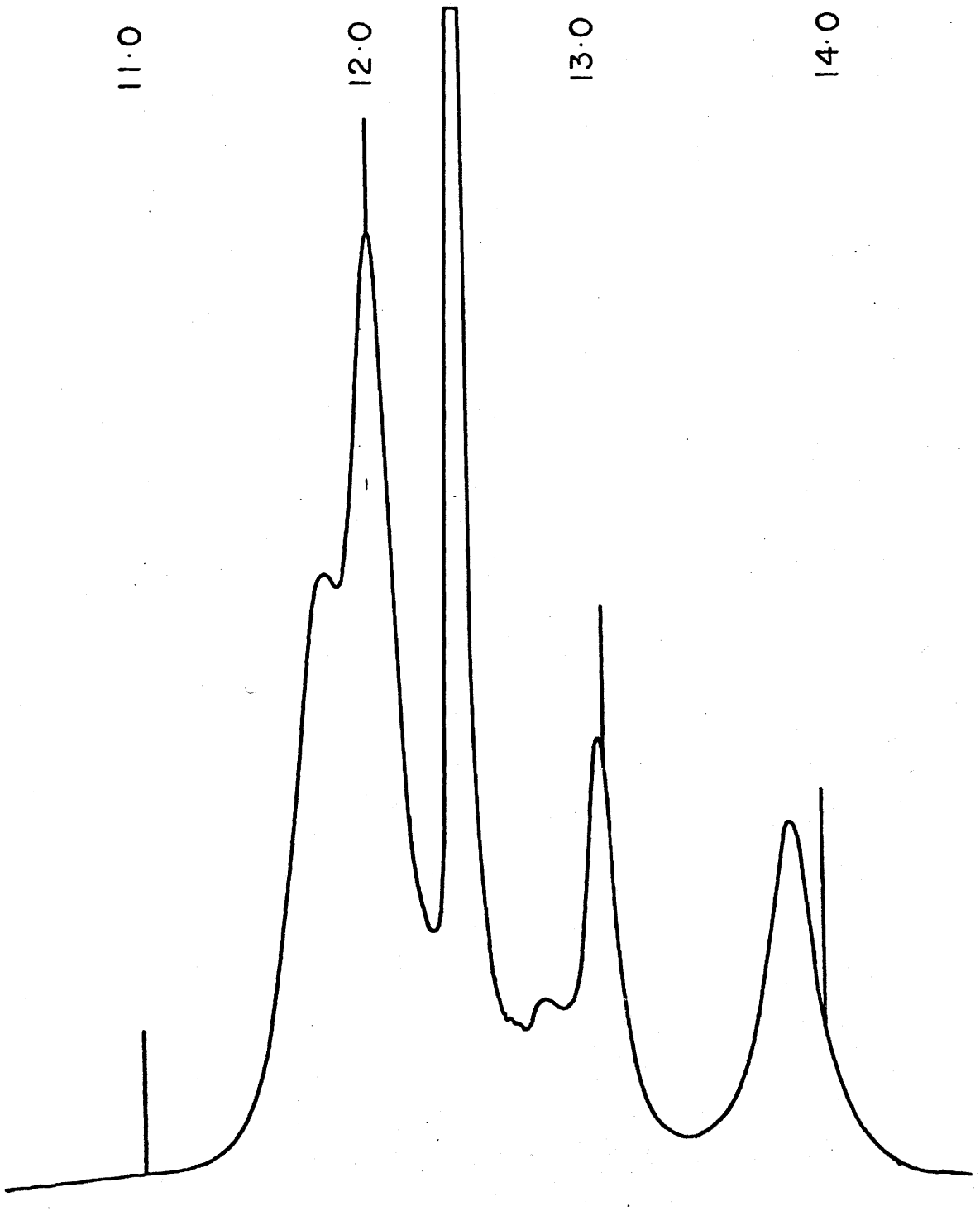

Fig. 4.8 Spectrum V obtained at temperature.
T = 1.3°K, ν = 34.810 GHz

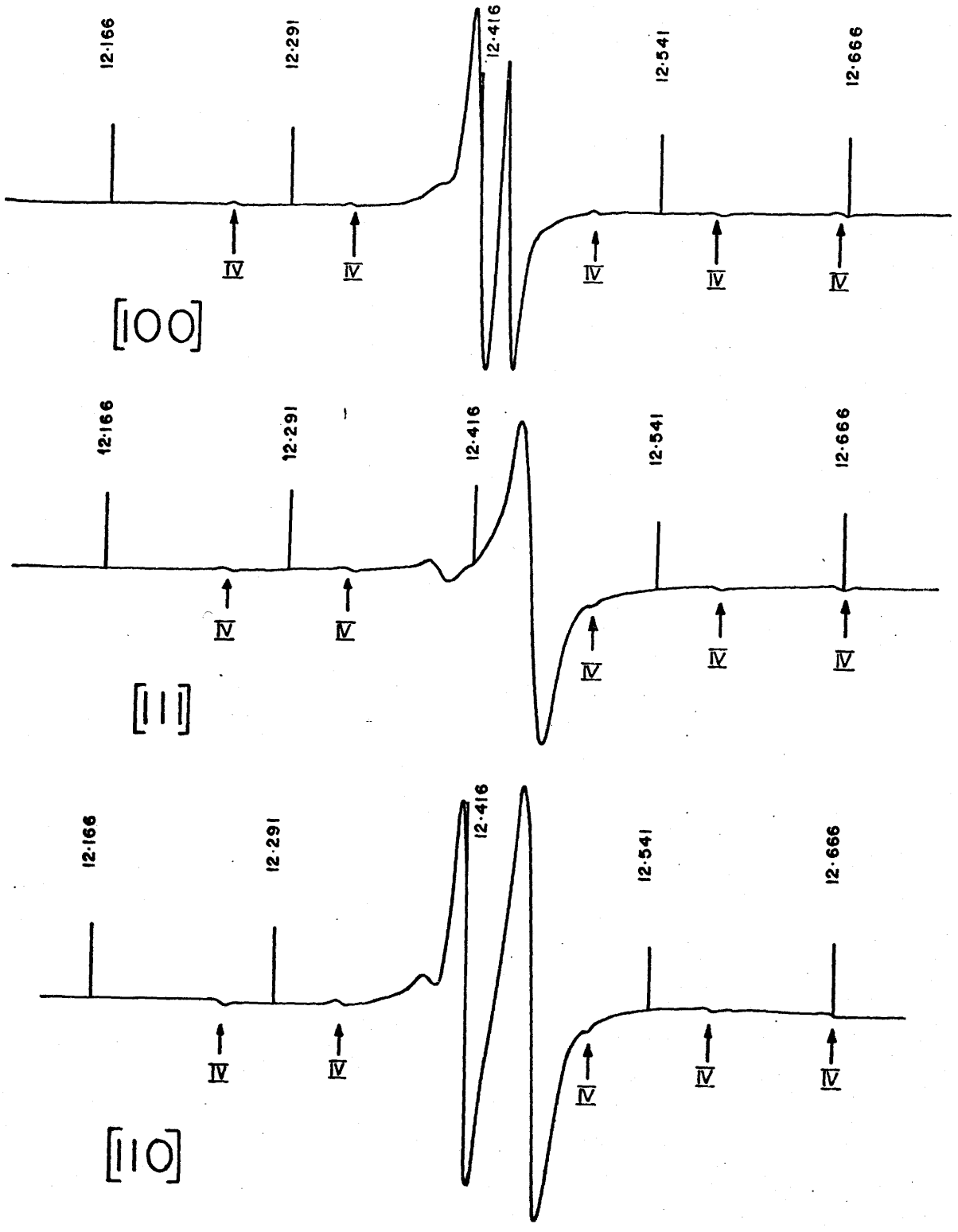

Fig. 4.9 Spectra I and IV with the magnetic field along the [100], [111], and [110] direction. ν = 34.876 GHz.

typically of the order 10^{-2} cm.$^{-1}$, (Bowers and Owen 1955). If one tries to explain the line separation of spectrum I at 0.8 cm and 3 cm wavelength respectively by a zero field splitting, this zero field splitting parameter in the fine structure Hamiltonian should also give rise to five fine structure lines if the spectrum was due to Fe^{3+}. In addition a spin Hamiltonian of the form

$$H = g\beta\vec{H}\cdot\vec{S} + D\{S_z^2 - \frac{1}{3}S(S+1)\} + E(S_x^2 - S_y^2) \qquad (4.1)$$

(Pake 1962) which holds for rhombic symmetry or

$$H = g\beta H\cdot S + \frac{1}{6}a\{S_x^4 + S_y^4 + S_z^4 - \frac{1}{5}S(S+1)(3S^2 + 3S-1)\} \qquad (4.2)$$

(Low 1960) which holds for cubic symmetry, yields an angular dependence of the transition lines which, when plotted out, give curves which lie nearly symmetrical about a center line which corresponds nearly to the free electron resonance value of the magnetic field. However, as can be seen from Figures 4.1, 4.2 and 4.3, neither plots show five lines with this characteristic angular dependence. Therefore, the possibility of attributing spectrum I to the fine structure of Fe^{3+} was ruled out.

Other interactions which have an angular dependence are the hyperfine and quadrupole interactions. Their angular dependence for $\Delta M = \pm 1$ transitions are for axially symmetric systems (Bleaney 1951):

$$Km + \frac{B^2}{4g\beta H_o}\left(\frac{A^2 + K^2}{K^2}\right)\{I(I+1) - m^2\} +$$

$$\frac{B^2}{2g\beta H_o}\,\frac{A}{K}\,m\,(2M+1) + \frac{m^2}{2g\beta H_o}\left(\frac{A^2-B^2}{K}\right)\left(\frac{g_\parallel g_\perp}{g^2}\right)^2 \sin^2\theta\cos^2\theta$$

$$+ \frac{Q\cos^2\theta\sin^2\theta}{2K\,M(M-1)}\left(\frac{ABg_\parallel g_\perp}{K^2 g^2}\right) m\,\{4I(I+1) - 8m^2 - 1\}$$

$$- \frac{Q^2\sin^4\theta}{8KM(M-1)}\left(\frac{Bg_\perp}{Kg}\right)^4 m\,\{2I(I+1) - 2m^2 - 1\} \qquad (4.3)$$

where $K^2g^2 = A^2g_\parallel^2\cos^2\theta + B^2g_\perp^2\sin^2\theta$ and A, B and $g_\parallel$, $g_\perp$ are the components of the hyperfine and fine structure tensor respectively. M and m are the electronic and nuclear magnetic quantum numbers and θ is the angle between the axis of axial symmetry and the magnetic field. Clearly the expression for the line separation between two hyperfine lines obtained from (4.3) would contain the terms

$$-\frac{B^2}{2g\beta H_o}\left(\frac{A^2+K^2}{K^2}\right)\left(m - \frac{1}{2}\right) + \frac{B^2}{2g\beta H_o}\,\frac{A}{K}\,(2M+1)$$

$$+ \frac{1}{g\beta H_o}\left(\frac{A^2-B^2}{K}\right)^2\left(\frac{g_\parallel g_\perp}{g^2}\right)^2 \sin^2\theta\cos^2\theta\,\left(m - \frac{1}{2}\right) \qquad (4.4)$$

which all vary as $\frac{1}{H}$ and could explain the difference in the 0.8 cm and 3 cm line separations. Again Fe has to be ruled out because Fe^{56} has no nuclear spin and a natural abundance of 98% whereas Fe^{57} has only a nuclear magnetic moment of less than 0.05 nuclear magnetons.

Another possibility is to postulate a defect center which has a non-zero magnetic moment such as a trapped electron or hole located at symmetry related sites with each site giving rise to one of the curves shown in Figures 4.1, 4.2 and 4.3. This however, seems unlikely since

spectrum I remained unaffected by the heat treatment described in section 1.

Spectra II, III, and IV

Since II and III disappear upon heat treatment it is difficult to attribute their origin to a paramagnetic impurity unless one postulates at the same time a change in the oxidation state of the impurity as a result of the heat treatment e.g. $Fe^{3+} + e^{-} \rightarrow Fe^{2+}$ and Fe^{2+} can only be observed at low temperatures. Hence the Fe^{3+} spectrum would disappear.

A more likely possibility is to postulate a trapped "defect center" for the following reason: When Mn^{2+} enters substitutionally as an impurity, the most likely location would be an Al^{3+} site since the chlorine and sodium atoms are usually ionically bound and hence not easily removed from the lattice. This process would require charge compensation in the form of introducing a defect of one positive charge by removing one electronic charge for every Mn^{2+} ion which is substituted. With these assumptions one could describe spectra II, III and IV using models similar to those used by Watkins (1959) to interpret the spectra of Mn^{2+} in alkali chlorides. Spectra II and III would then be identified as two separate sets of five fine structure lines each of which arise from the ground state $^{6}S_{5/2}$ of Mn^{2+}. In both cases the charge compensating defect is near the Mn^{2+} ion causing a strong anisotropy of the local crystal field. The site of this defect is nearer to the Mn^{2+} ion in the case of spectrum III than in the case of spectrum II hence

causing a largersplitting in III. The absence of hyperfine structure could be explained by exchange narrowing. Upon heat treatment the defects diffuse randomly throughout the crystal leaving the Mn^{2+} ion largely isolated in a predominantly cubic environment, so that the resulting spectrum IV displays well resolved hyperfine structure but no fine structure. Clearly the intensity of IV must increase since the total integrated intensity of II, III and IV must be the same before and after the heat treatment.

With this model in mind it was attempted to fit spectrum III to an orthorhombic spin Hamiltonian. The Al site has normally a distorted tetrahedral environment but due to the nearby defect center the symmetry of the spin Hamiltonian could be as low as orthorhombic. The Hamiltonian for rhombic symmetry is given by 4.1 and by writing down how this Hamiltonian transforms under rotation and by carrying out a second order perturbation calculation for the transformed Hamiltonian one obtains for transitions $\Delta M = \pm 1$ the following transition frequencies:

$$
\begin{aligned}
h\nu = {} & g\beta H_o + (M - \tfrac{1}{2}) \left[D(3\cos^2\theta - 1) - 3E(\cos^2\theta - 1)\cos 2\phi\right] \\
& + \left[(D - E\cos 2\phi)^2 (\sin\theta\cos\theta)^2 + (E\sin 2\phi)^2 \sin^2\theta\right] \\
& \cdot \left[\frac{1}{2g\beta H_o}\{4S(S+1) - 24M(M-1) - 9\}\right] \\
& + \left[\{D\sin^2\theta + E\cos 2\phi\,(1 + \cos^2\theta)\}^2 + 4\{E\cos\theta\cos 2\phi\}^2\right] \\
& \cdot \frac{1}{8g\beta H_o}\left[2S(S+1) - 6M(M-1) - 3\right]
\end{aligned}
\qquad (4.5)
$$

where the g-tensor has been assumed to be isotropic, which is generally true for S-states. D and E are the crystal field parameters and θ and ϕ are the polar and azimuthal angles which locate the magnetic field with respect to the magnetic axes.

The Al sites are located on the {100} cube faces with position co-ordinates $(0, \frac{1}{2}, \frac{1}{4})$ and all points generated from this site by the space group $P\bar{4}3m$. The twofold axes contained in each cubic face intersect both the center of the cube face and two Al sites. Therefore one magnetic axis, say the z axis, is constrained to lie along the twofold axis. The only other constraint on the magnetic axes is that they have to form a righthanded orthogonal axes triplet. Therefore, without loss of generality, it can be assumed that the x-axis encloses an angle γ with the (100) planes. Thus when the magnetic field H is parallel to the [100] direction there are three inequivalent Al sites each of which has a magnetic axes triplet associated with it. If the three sites are denoted by 1, 2 and 3 the magnetic field direction is described by the following angles:

$$\text{for site 1:} \quad \theta = 0;$$

$$\text{for site 2:} \quad \theta = 90^\circ; \quad \phi = \gamma;$$

$$\text{for site 3:} \quad \theta = 90^\circ; \quad \phi = \gamma - 90^\circ;$$

where γ is an adjustable parameter.

The resonant magnetic field is obtained from 4.5 by substituting the proper values for θ and ϕ:

for site 1:

$$H = H_o + (M - \tfrac{1}{2})\, 2D \tag{4.6}$$

for site 2:

$$H = H_o + (M - \tfrac{1}{2})\,[-D + 3E\cos 2\gamma] + \frac{E^2 \sin^2 2\gamma}{2H_o}\,[26 - 24M(M-1)] + \frac{(D + E\cos 2\gamma)^2}{8H_o}\,[\tfrac{29}{2} - 6M(M-1)] \tag{4.7}$$

for site 3:

$$H = H_o + (M - \tfrac{1}{2})\,[-D - 3E\cos 2\gamma] + [E^2 \sin^2 2\gamma]\,[\frac{26 - 24\,M(M-1)}{2H_o}] + \frac{[D - E\cos 2\gamma]^2}{8H_o}\,[\tfrac{29}{2} - 6M(M-1)] \tag{4.8}$$

The values of the observed line positions are given in Table 4.2.

Table 4.2

<100> directions	<110> directions
13.799 [kilogauss]	
13.100 "	13.085 [kilogauss]
12.515* "	11.941 "
11.941 "	
11.223 "	

* This value was obtained by taking the arithmetic mean of the other values.

Clearly the largest line separation occurs for site 1. Substituting the observed H values into 4.6, one obtains for transitions $M = \frac{5}{2} \rightarrow M = \frac{3}{2}$

$$13.799 = 12.515 + 4D \qquad \text{[this is correct to second order!]}$$

$$D = 0.321 \text{ [kilogauss]}$$

The next largest splitting was associated with the $M = \frac{5}{2} \rightarrow M = \frac{3}{2}$ transition of site 2 in favour of the $M = \frac{3}{2} \quad M = \frac{1}{2}$ transition of site 1 since there are 8 sites of type 2 and only 4 sites of type 1 which means that their intensities are in the ratios 2:1.

Substituting into 4.7 one obtains to first order:

$$13.100 = 12.515 + 0.642 + 6E \cos 2\gamma$$

$$\therefore E \cos 2\gamma = -0.001 \text{ [kilogauss]} .$$

For the magnetic field parallel to [110] the angles θ, ϕ become for the three non-equivalent sites:

site 1: $\theta = 90°$; $\quad \phi = \gamma - 45°$;

site 2: $\theta = 135°$; $\quad \phi = \gamma - 90°$;

sitr 3: $\theta = 135°$; $\quad \phi = \gamma - 180°$;

Clearly site 1 gives the largest splitting as can be seen from 4.5

$\therefore$for site 1

$$H = H_o + (M - \tfrac{1}{2}) [-D + 3E \sin 2\gamma]$$

$$+ \frac{E^2 \cos^2 2\gamma}{2H_o} [26 - 24 M(M - 1)]$$

$$+ \frac{(D + E \sin 2\gamma)^2}{8H_o} [\tfrac{29}{2} - 6M(M - 1)]$$

Substituting the observed H values for the transition

$$M = \frac{5}{2} \rightarrow M = \frac{3}{2}$$ one obtains:

$$13.085 = 12.515 + 2 \times 0.32 + 6E \sin 2\gamma$$

$$\therefore E \sin 2\gamma = -0.012$$

Since $E^2 \sin^2 2\gamma + E^2 \cos^2 2\gamma = E^2$

one obtains $E = -0.012$ [kilogauss] and $\gamma = 45°$.

The small value of E justifies the use of the first order equations in E since all magnetic field values are only 0.1% accurate.

To obtain the expression for the angular variation of the line positions of site 1 in a plane of type {100} one observes that θ is the angle of rotation, whereby $\theta = 0$ for H parallel to the [100] direction, and $\phi = 45°$.

For $M = \pm\frac{5}{2} \rightleftarrows M = \pm \frac{3}{2}$ transitions one obtains

$$H = H_o \pm 2[D(3 \cos^2 \theta - 1)] + \frac{32 E^2 \sin^2 \theta}{H_o}$$

$$- \frac{[D^2 \sin^4 \theta + 4 E^2 \cos^2 \theta]}{H_o} =$$

$$H_o \pm 2D(3 \cos^2 \theta - 1) - \frac{D^2 \sin^4 \theta}{H_o}$$

to within the experimental error.

Similarly for planes of type {110} θ is the angle of rotation and $\phi = 0$ for site 1. The transitions $M = \pm \frac{5}{2} \rightleftarrows M = \pm \frac{3}{2}$ are given by

$$H = H_o \pm 2D(3\cos^2\theta - 1) - \frac{32\,D^2\sin^2\theta\cos^2\theta}{H_o}$$

$$- \frac{[D^2\sin^4\theta + 4E^2\cos^2\theta]}{H_o}$$

$$= H_o \pm 2D(3\cos^2\theta - 1) - \frac{32\,D^2\sin^2\theta\cos^2\theta}{H_o}$$

$$- \frac{D^2\sin^4\theta}{H_o} \quad \text{to within the experimental error.}$$

When the calculated values of D and E are substituted one obtains the curves which are traced out by the solid lines in Figures 4.6 and 4.7.

It is seen from Figures 4.6 and 4.7 that the models used to describe spectrum III are in qualitative agreement with the experimental results. The poor quantitative agreement displayed in Fig. 4.7 in the neighbourhood of the [011] direction could be due to the truncation of the spin Hamiltonian after the quadratic terms in the effective spin S. In the presence of a cubic crystalline field component, however, the fourth order terms in S contribute significantly to the angular variation of the spectra. It is unlikely that a higher order perturbation calculation would have remedied the situation in view of the already small contributions of the second order terms in $\frac{E^2}{H_o}$ and $\frac{D^2}{H_o}$. The experimental points in Fig. 4.6 in the neighbourhood of the 45° and 135° direction are interpreted as being due to sites 2 and 3 whereas the solid line only applies to site 1. According to formulae 4.7 and 4.8 sites 2 and 3 give line positions at $H = H_o \pm 2D = 13.15$ and 11.87 kilogauss to first order for $\pm\frac{5}{2} \nrightarrow \pm\frac{3}{2}$ transitions, which corresponds to the observed values in these directions.

3. Conclusion

It is seen that the E. P. R. signals in sodalite can be divided into five spectra each of which requires a separate analysis. Of these five spectra spectrum IV is certain to arise from manganese which is contained in the sodalite samples as an impurity. The characteristic blue colour of sodalite crystals does not appear to be related to any of the four room temperature spectra studied. It was established that the E. P. R. signals change upon heat treatment and the room temperature signals differ greatly from those observed at 1.3°K.

Further experiments are necessary to determine uniquely the origin of the various spectra. These should include studies on samples with different manganese concentrations. Also by quenching samples at different temperatures below 900°C it should be possible to determine if the decrease in intensity of spectrum II leads to a simultaneous increase in intensity of spectrum IV. The postulate of the $\frac{1}{H}$ dependence of the line separations of spectrum I could be verified by using 4 mm microwave radiation.

BIBLIOGRAPHY

1. A. Abragam and M. H. L. Pryce (1951), Proc. Roy. Soc. (London), A 205, 135.
2. T. F. W. Barth (1932), Zeit. f. Krist. 74, 213.
3. H. A. Bethe (1929), Ann. Physik 3, 133
4. V. B. Bleaney (1951), Phil. Mag. 42, 441
5. K. D. Bowers and J. Owen (1955), Repts. Progr. in Phys. 18, 304.
6. G. Feher (1957), Bell System Tech. J. 36, 449.
7. J. S. Leung (1964), Master's Thesis, McMaster University.
8. W. Low (1960), Paramagnetic Resonance in Solids, p. 116.
9. O. K. Mel'nikov (1965), Sov. Phy. Crys. 10, No. 2, 216.
10. G. E. Pake (1962), Paramagnetic Resonance, p. 69.
11. L. Pauling (1930), Zeit. f. Krist. 74, 213.
12. Yu. V. Shaldin (1966), Sov. Phy. Crys. 10, No. 4, 484.
13. B. Smaller (1951), Phys. Rev. 83, 816.
14. G. D. Watkins (1959), Phys. Rev. 113, 79.